AIAA JOURNAL
Vol. 31, No. 12, December 1993

Thermoviscoelastic Analysis of Delamination Onset and Free Edge Response in Laminated Composites

Sung Yi*
University of Illinois at Urbana-Champaign, Urbana, Illinois 61801

Time-dependent boundary-layer stress fields near free edges in epoxy matrix composite laminates due to mechanical and hygroscopic loadings are analyzed using finite element methods. The numerical formulation is based on Laplace transforms rather than direct time integrations in order to improve the accuracy of solutions and to save extensive computational time and memory storage. Numerical results for the time-dependent free edge stresses in $(45/-45)_s$ kevlar/epoxy laminates subjected to moisture absorption cycles or time-varying uniaxial extensions are presented. The delamination initiations in $(15/-15)_s$ T300/934 graphite/epoxy laminate are predicted as functions of time and loading history by using a newly modified Quadratic Delamination Criterion to account for time-dependent strengths.

Introduction

DELAMINATION between each layer is a common failure mode in laminated composites. Interlaminar stresses which exist near free edges of laminates influence the delamination onset and growth and arise mainly due to mismatches in layer properties. For this reason, many analytical and numerical studies[1-10] have been undertaken to evaluate free edge stresses and to experimentally determine their existence. Several investigators[2,5,9] have also studied thermal or hygroscopic interlaminar stresses in graphite/epoxy laminates. However, these elastic approaches do not accurately predict the residual stress and strain fields in epoxy matrix composites since the material properties of epoxy matrices are strongly time-dependent. The epoxy matrix exhibits degradation of material mechanical properties at elevated temperatures and/or in the presence of moisture.[11-13] Hygrothermal expansions induce residual stresses in a composite laminate which may result in delaminations and subsequent structural failures.[14-16]

Since the interlaminar stresses at the free edge of laminates are mathematically singular and since peak values of those stresses calculated by finite element methods are dependent on mesh size, the maximum values of those stresses cannot be accurately used for failure analyses. Thus, delamination has been predicted by using the strain-energy release rate approach and other failure criteria. O'Brien[3] suggested the strain-energy release rate approach for predicting initiation and growth of delaminations. Kim and Soni[6] also studied the onset of delaminations by using the average stress criterion which had been proposed by Whitney and Nuismer[33] for failure analyses of notched composite plates. The average stress criterion assumes that the initiation of delamination occurs when the average values of interlaminar stresses over a critical length reach prescribed interlaminar strengths. A more appropriate failure criterion for predicting the onset of delamination based upon the average interlaminar stress fields is the Quadratic Delamination Criterion suggested by Brewer and Lagace.[8]

In the present study, the time-dependent stress and strain fields near free edges of composite laminates are evaluated using the finite element method developed by Hilton and Yi[17,18] for efficient analyses of long-term predictions of time-dependent deformations and stresses in linear anisotropic thermoviscoelastic composite materials which are subjected to mechanical, thermal, and hygroscopic loads. The initiation of delaminations in the presence of boundary-layer stress singularities is also predicted by incorporating the modified Quadratic Delamination Criterion as a function of load and environment history.

Governing Equations For Generalized Plane Strain Problem

The laminate depicted in Fig. 1 is assumed to be long in the x_1 direction, which corresponds to generalized plane strain conditions. Consequently, the strain and stress fields in the laminate are independent of the x_1 coordinate. The geometry, material properties, and loads are symmetric with respect to the $x_2 - x_3$ axes (middle plane). The displacement field for this problem can be described as

$$u = x_1 \cdot \epsilon_1(t) + U(x_2, x_3, t) \tag{1a}$$

$$v = V(x_2, x_3, t) \tag{1b}$$

$$w = W(x_2, x_3, t) \tag{1c}$$

where u, v, and w are, respectively, displacements in the x_1, x_2, and x_3 directions and $\epsilon_1(t)$ is an applied uniform axial strain in the x_1 direction. It is unknown when the laminate is subjected to axial tensile forces or hygrothermal loadings.

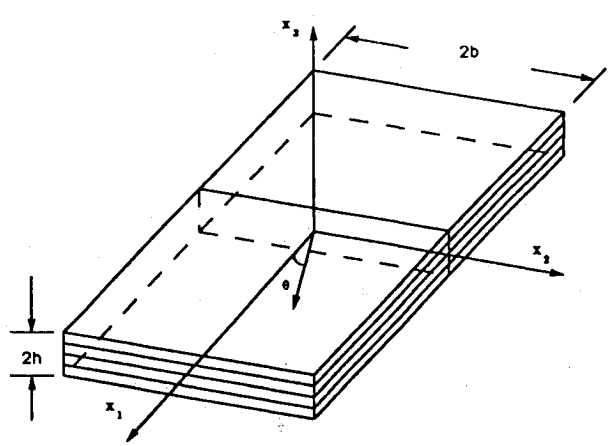

Fig. 1 Coordinate and geometry of a laminate under the generalized plane strain condition.

Presented as Paper 91-0962 at the AIAA/ASME/ASCE/AHS/ASC 32nd Structures, Structural Dynamics, and Materials Conference, Baltimore, MD, April 8-10, 1991; received June 9, 1992; revision received April 10, 1993; accepted for publication April 13, 1993.

*Post-Doctoral Research Associate, National Center for Supercomputing Applications, 405 North Mathews.

The strain-displacement relationship in contracted notation is

$$\epsilon_x(x, t) = \epsilon_1(x, t) = \frac{\partial u}{\partial x_1} \tag{2a}$$

$$\epsilon_y(x, t) = \epsilon_2(x, t) = \frac{\partial v}{\partial x_2} \tag{2b}$$

$$\epsilon_z(x, t) = \epsilon_3(x, t) = \frac{\partial w}{\partial x_3} \tag{2c}$$

$$\gamma_{yz}(x, t) = \epsilon_4(x, t) = \frac{\partial v}{\partial x_3} + \frac{\partial w}{\partial x_2} \tag{2d}$$

$$\gamma_{xz}(x, t) = \epsilon_5(x, t) = \frac{\partial u}{\partial x_3} \tag{2e}$$

$$\gamma_{xy}(x, t) = \epsilon_6(x, t) = \frac{\partial u}{\partial x_2} \tag{2f}$$

where ϵ_i are engineering strains in the laminate coordinates and u, v, and w are displacements defined in Eq. (1).

The constitutive relationship for anisotropic linear hygrothermoviscoelastic materials can be expressed in condensed notation by the following hereditary integrals[19,20]:

$$\sigma_i(T, M, x, t) = \int_{-\infty}^{t} \bar{Q}_{ij}(T, M, t, \tau) \frac{\partial}{\partial \tau} [\epsilon_j(x, \tau) - \epsilon_j^*(x, \tau)]\, d\tau \tag{3}$$

where x are laminate coordinates, $\bar{Q}_{ij}$ are transformed relaxation moduli, σ_i are stress components at time t, and ϵ_j and ϵ_j^* are total strains and free hygrothermal strains, respectively. Note the above constitutive equations are not convolution integrals since material properties of epoxy matrix composites strongly depend upon temperature and/or moisture. The coefficients of hygrothermal expansions are assumed to be independent of time, temperature, and moisture. The free hygrothermal strains ϵ_j^* may then be expressed as

$$\epsilon_j^*(X, t) = \bar{\alpha}_j \Delta T(X, t) + \bar{\beta}_j \Delta M(X, t) \tag{4}$$

where $\bar{\alpha}_j$ and $\bar{\beta}_j$ are, respectively, thermal and hygroscopic expansion coefficients transformed with respect to the laminate coordinate system and ΔT and ΔM are temperature and moisture changes related to an unstressed reference state. Material properties of composites are dependent on temperature and/or moisture and exhibit time temperature/moisture shift characteristics. For hygrothermorheologically simple materials,[19,20] the relaxation moduli in the principal material coordinates can be represented in the form

$$Q_{ij}[T(X, t), M(X, t)] = Q_{ij}[T_r, M_r, \zeta_{ij}(X, t)] \tag{5}$$

where X are the principal material coordinates, the subscript r denotes reference conditions, and the ζ_{ij} are pseudo or reduced times, which are related to the shift functions a_{ij} by

$$\zeta_{ij}(X, t) = \int_0^t a_{ij}[T(X, \tau), M(X, \tau)]\, d\tau \tag{6}$$

Composite viscoelastic material properties can be determined from tensile relaxation experiments.[11-13] Experimental data for epoxy matrix composites show that E_{11} and ν_{12} are not sensitive to time, temperature, and moisture. The transverse modulus E_{22} and the shear modulus G_{12} have a similar time-dependent behavior. In the present study, Q_{11} is assumed to be time-independent since the x_1 direction is dominated by fibers and the other moduli such as Q_{12}, Q_{22}, and Q_{66} are assumed to have the same reduced times and shift functions. All ζ_{ij} in Eq. (6) are assumed identical and equal to ζ. This allows one to express the relaxation moduli in terms of Prony series such that

$$Q_{ij}(\zeta) = Q_{ij0} + \sum_{\rho=1}^{N} Q_{ij\rho} \exp(-\zeta/\lambda_\rho) \tag{7}$$

where the parameters λ_ρ are relaxation times, N is the number of terms in the series, and Q_{ij0} and $Q_{ij\rho}$ are time-independent and symmetric material property coefficients.

For computational purposes, Eq. (7) can be rewritten as

$$Q_{ij}(\zeta) = Q_{ij}^0 + Q_{ij}^t \sum_{\rho=1}^{N} \eta_\rho \cdot \exp(-\zeta/\lambda_\rho) \tag{8}$$

where

$$Q_{ij}^0 = Q_{ij0}, \quad Q_{ij}^t = \sum_{\rho=1}^{N} Q_{ij\rho}, \quad \text{and} \quad \eta_\rho = Q_{ij\rho}/Q_{ij}^t$$

The stress-strain relations then can be rewritten in the $x - \zeta$ plane as[19,20]

$$\hat{\sigma}_i(x, \zeta) = \int_{-\infty}^{\zeta} \hat{\bar{Q}}_{ij}[T_r, M_r, \zeta - \zeta'] \frac{\partial}{\partial \zeta'} [\hat{\epsilon}_j(x, \zeta') - \hat{\epsilon}_j^*(x, \zeta')]\, d\zeta' \tag{9}$$

where $\hat{\bar{Q}}_{ij}$ are the moduli in $x - \zeta$ plane, $\hat{\sigma}_i(x,\zeta) = \sigma_i(x,t)$, $\hat{\epsilon}_j(x,\zeta) = \epsilon_j(x,t)$, and $\hat{\epsilon}_j^*(x,\zeta) = \epsilon_j^*(x,t)$.

The introduction of these reduced times changes the constitutive equations to convolution ones in the $x - \zeta$ plane; however, x_i derivatives in the field equations take on new definitions, i.e.,

$$\left(\frac{\partial}{\partial x_i}\right)_t = \left(\frac{\partial}{\partial x_i}\right)_\zeta + \left(\frac{\partial \zeta}{\partial x_i}\right)_t \left(\frac{\partial}{\partial \zeta}\right)_x \tag{10}$$

Although the ζ derivatives with respect to x_i can be computed, their accuracy is low since the shift functions in Eq. (6) are experimentally determined. The present method avoids such pitfalls by determining all derivatives in the $x - t$ plane and then at later stages transforming the equations into the $x - \zeta$ plane.

Variational Principles

The variational functional for linear viscoelastic problems has been given by Gurtin[21] and in the absence of body forces the first variation is now extended to hygrothermoviscoelasticity as

$$\delta\pi = \int_V \int_{\tau'=-\infty}^{\tau'=t} \int_{\tau=-\infty}^{\tau=t-\tau'} \bar{Q}_{ij}[T_r, M_r, \zeta(x, t-\tau') - \zeta'(x, \tau)] \cdot \frac{\partial}{\partial \tau} \{\epsilon_i(x, \tau) - \epsilon_i^*(x, \tau)\}\, d\tau \cdot \frac{\partial \delta\epsilon_j(x, \tau')}{\partial \tau'}\, d\tau'\, dV - \int_{S_T} \int_{\tau'=-\infty}^{\tau'=t} \Omega_i(t-\tau') \frac{\partial \delta u_i(x, \tau')}{\partial \tau'}\, d\tau'\, dS_T = 0 \tag{11}$$

where V is the volume of viscoelastic solid, S_T is the surface on which tractions Ω_i are applied, and u_i are the displacements.

Finite Element Formulation in Laplace Domain

The finite element equilibrium equations for analyses of viscoelastic composite laminates are derived from the constitutive integral equations and variational principles. Four-node rectangular elements are used in the present study and the displacement field within each element is represented by bilinear interpolation functions. The displacement equation related to the nodal degrees of freedom can be written as

$$\begin{Bmatrix} U(x_2, x_3, t) \\ V(x_2, x_3, t) \\ W(x_2, x_3, t) \end{Bmatrix} = [L(x_2, x_3)]\, \{q(t)\} \tag{12}$$

where $[L(x_2, x_3)]$ is the bilinear shape function and $\{q(t)\}$ is the nodal displacement vector:

$$\{q(t)\} = \lfloor q_1\ q_2\ q_3\ q_4\ q_5\ q_6\ q_7\ q_8\ q_9\ q_{10}\ q_{11}\ q_{12} \rfloor^T$$

When Eq. (12) is substituted into Eq. (1), the following expressions for the displacement field within an element are obtained:

$$\begin{Bmatrix} u \\ v \\ w \end{Bmatrix} = \begin{Bmatrix} x_1 \cdot \epsilon_1(t) + U \\ V \\ W \end{Bmatrix} = [\boldsymbol{J}\boldsymbol{L}] \begin{Bmatrix} \epsilon_1(t) \\ q(t) \end{Bmatrix} \tag{13}$$

where $\{\boldsymbol{J}\}$ is $\lfloor x_1\ 0\ 0 \rfloor^T$.

Differentiating Eq. (13) with respect to x_i results in the following strain-displacement relationship:

$$\{\epsilon(t)\} = \begin{bmatrix} \mathbf{1} & \mathbf{0} \\ \mathbf{0} & \boldsymbol{B}(x_2, x_3) \end{bmatrix} \begin{Bmatrix} \epsilon_1(t) \\ q(t) \end{Bmatrix} \tag{14}$$

where $[\boldsymbol{B}]$ is a 5×12 matrix.

By substituting Eqs. (13) and (14) into the variational expression Eq. (11), the following finite element equilibrium equations can be obtained for each element:

$$\int_{-\infty}^{t} k_{mn}(\zeta - \zeta') \frac{\partial q_n'(\tau)}{\partial \tau}\, d\tau = f_m(t) + f_m^r(t) \tag{15}$$

where $f_m^r(t)$ are element residual nodal forces and $f_m(t)$ are reactive nodal forces which are unknown at this stage. When only ϵ_1 is applied to a laminate, the nodal displacement vector $q_n'(\tau)$ is

$$\{q_n'(\tau)\} = \{q(\tau)\} \tag{16}$$

but for hygrothermal loading, it becomes

$$\{q_n'(\tau)\} = \begin{Bmatrix} q(\tau) \\ \epsilon_1(\tau) \end{Bmatrix} \tag{17}$$

In the case of only mechanical loading, the element stiffness matrix k_{mn} and the element residual nodal force vector f_m^r can be expressed as

$$\begin{aligned} k_{mn}(\zeta - \zeta') &= \iint_{A^e} B_{im} \bar{Q}_{(i+1)(j+1)}(\zeta - \zeta') B_{jn}\, dx_2\, dx_3 \\ &= k_{mn}^0 + k_{mn}^t \sum_{\rho=1}^{N} \eta_\rho \cdot \exp\left[-(\zeta - \zeta')/\lambda_\rho\right] \end{aligned} \tag{18}$$

and

$$\begin{aligned} f_m^r(t) &= -\int_{\tau=-\infty}^{\tau=t} \iint_{A^e} B_{im} \bar{Q}_{i1}(\zeta - \zeta') \frac{\partial \epsilon_1(\tau)}{\partial \tau}\, d\tau\, dx_2\, dx_3 \\ &= \left\{ f_m^0 + f_m^t \sum_{\rho=1}^{N} \eta_\rho \cdot \exp\left[-\zeta/\lambda_\rho\right] \right\} \epsilon_1(0) \\ &\quad + \int_{\tau=0}^{\tau=t} \left\{ f_m^0 + f_m^t \sum_{\rho=1}^{N} \eta_\rho \cdot \exp\left[-(\zeta - \zeta')/\lambda_\rho\right] \right\} \frac{\partial \epsilon_1(\tau)}{\partial \tau}\, d\tau \end{aligned} \tag{19}$$

where $i, j = 1, 2, \ldots, 5$, and $m, n = 1, 2, \ldots, 12$; and A^e designates the area of the element and

$$k_{mn}^0 = \iint_{A^e} B_{im} \bar{Q}_{(i+1)(j+1)}^0 B_{jn}\, dx_2\, dx_3 \tag{20a}$$

$$k_{mn}^t = \iint_{A^e} B_{im} \bar{Q}_{(i+1)(j+1)}^t B_{jn}\, dx_2\, dx_3 \tag{20b}$$

$$f_m^0 = -\iint_{A^e} B_{im} \bar{Q}_{i1}^0\, dx_2\, dx_3 \tag{20c}$$

$$f_m^t = -\iint_{A^e} B_{im} \bar{Q}_{i1}^t\, dx_2\, dx_3 \tag{20d}$$

When the laminates are subjected to thermal and/or hygroscopic loads, the element stiffness matrix k_{mn} is a 13×13 matrix. The 12×12 components of this matrix are the same as those described in Eq. (18) and the additional components are

$$k_{m,13}(\zeta - \zeta') = \iint_{A^e} B_{im} \bar{Q}_{i1}(\zeta - \zeta')\, dx_2\, dx_3 \tag{21a}$$

$$k_{13,m}(\zeta - \zeta') = \iint_{A^e} \bar{Q}_{1i}(\zeta - \zeta') B_{im}\, dx_2\, dx_3 \tag{21b}$$

$$k_{13,13}(\zeta - \zeta') = \iint_{A^e} \bar{Q}_{11}(\zeta - \zeta')\, dx_2\, dx_3 \tag{21c}$$

The residual nodal force vector due to hygrothermal load becomes

$$\begin{aligned} \{f_n^r(t)\} = \iint_{A^e} \int_{\tau=-\infty}^{\tau=t} \Bigg\{ & B_{in} \bar{Q}_{(i+1)(j+1)}(\zeta - \zeta') \cdot \frac{\partial \epsilon_{(j+1)}^*(\tau)}{\partial \tau} \\ & + B_{in} \bar{Q}_{i1}(\zeta - \zeta') \frac{\partial \epsilon_1^*(\tau)}{\partial \tau} \Bigg\}\, d\tau\, dx_2\, dx_3 \end{aligned} \tag{22}$$

and

$$\begin{aligned} f_{13}^r(t) = \iint_{A^e} \int_{\tau=-\infty}^{\tau=t} \Bigg\{ & \bar{Q}_{1i}(\zeta - \zeta') \frac{\partial \epsilon_{(j+1)}^*(\tau)}{\partial \tau} \\ & + \bar{Q}_{11}(\zeta - \zeta') \frac{\partial \epsilon_1^*(\tau)}{\partial \tau} \Bigg\}\, d\tau\, dx_2\, dx_3 \end{aligned} \tag{23}$$

By using the exponential series for Q_{ij} given in Eq. (8), the residual force vector in Eqs. (22) and (23) can be rewritten as

$$\begin{aligned} f_n^r(t) &= \{f_n^{\alpha 0} + f_n^{\alpha t} \sum_{\rho=1}^{N} \eta_\rho \cdot \exp\left[-\zeta/\lambda_\rho\right]\} \cdot \Delta T(0) \\ &\quad + \{f_n^{\beta 0} + f_n^{\beta t} \sum_{\rho=1}^{N} \eta_\rho \cdot \exp\left[-\zeta/\lambda_\rho\right]\} \cdot \Delta M(0) \\ &\quad + \int_{\tau=0}^{\tau=t} \Bigg\{ \{f_n^{\alpha 0} + f_n^{\alpha t} \sum_{\rho=1}^{N} \eta_\rho \cdot \exp\left[-(\zeta - \zeta')/\lambda_\rho\right]\} \cdot \frac{\partial \Delta T(\tau)}{\partial \tau} \\ &\quad + \{f_n^{\beta 0} + f_n^{\beta t} \sum_{\rho=1}^{N} \eta_\rho \cdot \exp\left[-(\zeta - \zeta')/\lambda_\rho\right]\} \cdot \frac{\partial \Delta M(\tau)}{\partial \tau} \Bigg\} \cdot d\tau \end{aligned} \tag{24}$$

and

$$\begin{aligned} f_{13}^r(t) &= \{f_{13}^{\alpha 0} + f_{13}^{\alpha t} \sum_{\rho=1}^{N} \eta_\rho \cdot \exp\left[-\zeta/\lambda_\rho\right]\} \cdot \Delta T(0) \\ &\quad + \{f_{13}^{\beta 0} + f_{13}^{\beta t} \sum_{\rho=1}^{N} \eta_\rho \cdot \exp\left[-\zeta/\lambda_\rho\right]\} \cdot \Delta M(0) \\ &\quad + \int_{\tau=0}^{\tau=t} \Bigg\{ \{f_{13}^{\alpha 0} + f_{13}^{\alpha t} \sum_{\rho=1}^{N} \eta_\rho \cdot \exp\left[-(\zeta - \zeta')/\lambda_\rho\right]\} \cdot \frac{\partial \Delta T(\tau)}{\partial \tau} \\ &\quad + \{f_{13}^{\beta 0} + f_{13}^{\beta t} \sum_{\rho=1}^{N} \eta_\rho \cdot \exp\left[-(\zeta - \zeta')/\lambda_\rho\right]\} \cdot \frac{\partial \Delta M(\tau)}{\partial \tau} \Bigg\} \cdot d\tau \end{aligned} \tag{25}$$

where

$$f_n^{\alpha 0} = \iint_{A^e} \{B_{in} \bar{Q}_{(i+1)(j+1)}^0 \bar{\alpha}_{(j+1)} + B_{in} \bar{Q}_{i1}^0 \bar{\alpha}_1\}\, dx_2\, dx_3 \tag{26a}$$

$$f_n^{\beta 0} = \iint_{A^e} \{B_{in} \bar{Q}_{(i+1)(j+1)}^0 \bar{\beta}_{(j+1)} + B_{in} \bar{Q}_{i1}^0 \bar{\beta}_1\}\, dx_2\, dx_3 \tag{26b}$$

$$f_{13}^{\alpha 0} = \iint_{A^e} \{\bar{Q}_{1i}^0 \bar{\alpha}_{(i+1)} + \bar{Q}_{11}^0 \bar{\alpha}_1\}\, dx_2\, dx_3 \tag{26c}$$

$$f_{13}^{\beta^0} = \int\int_{A^e} \{\bar{Q}_{1i}^0 \bar{\beta}_{(i+1)} + \bar{Q}_{11}^0 \bar{\beta}_1\}\, dx_2\, dx_3 \tag{26d}$$

$$f_n^{\alpha^t} = \int\int_{A^e} \{B_{in}\bar{Q}_{(i+1)(j+1)}^t \bar{\alpha}_{(j+1)} + B_{in}\bar{Q}_{i1}^t \alpha_1\}\, dx_2\, dx_3 \tag{26e}$$

$$f_n^{\beta^t} = \int\int_{A^e} \{B_{in}\bar{Q}_{(i+1)(j+1)}^t \bar{\beta}_{(j+1)} + B_{in}\bar{Q}_{i1}^t \bar{\beta}_1\}\, dx_2\, dx_3 \tag{26f}$$

$$f_{13}^{\alpha^t} = \int\int_{A^e} \{\bar{Q}_{1i}^t \bar{\alpha}_{(i+1)} + \bar{Q}_{11}^t \bar{\alpha}_1\}\, dx_2\, dx_3 \tag{26g}$$

$$f_{13}^{\beta^t} = \int\int_{A^e} \{\bar{Q}_{1i}^t \bar{\beta}_{(i+1)} + \bar{Q}_{11}^t \bar{\beta}_1\}\, dx_2\, dx_3 \tag{26h}$$

In the $x - \zeta$ plane, the assemblage of element contributions over the entire domain yields the following convolution integral equations:

$$\int_{-\infty}^{\zeta} \hat{K}_{mn}(\zeta - \zeta') \frac{\partial \hat{u}_n(\zeta')}{\partial \zeta'}\, d\zeta' = \hat{F}_m(\zeta) + \hat{F}_m^r(\zeta) \tag{27}$$

where $\hat{F}_m(\zeta) = F_m(t)$; $\hat{F}_m^r(\zeta) = F_m^r(t)$; $m, n = 1, 2, \ldots, NDT$; and NDT is the total number of degrees of freedom. In the above, $\hat{K}_{mn}$ is the global stiffness matrix, $\hat{u}_n$ is the global vector of nodal displacements, and $\hat{F}_m$ and $\hat{F}_m^r$ are global nodal force vectors due to applied tractions $\bar{T}$ and ϵ_1 and/or hygrothermal loading, respectively.

Since the finite element equilibrium Eq. (27) is expressed in hereditary integral form, direct integration requires extensive memory storage and consumes large amounts of real computational time. Thus, many numerical schemes for the analysis of viscoelastic boundary-value problems have been proposed.[10, 22-25] Using finite difference recurrence relationships, Zak[22] developed a numerical procedure to analyze isotropic linear viscoelastic solid propellant materials undergoing mechanical and thermal deformations. This method has the advantage of saving extensive memory storage since it requires storage of only the previous time solutions instead of all of the solutions throughout the entire loading time history. Taylor et al.[23] adopted Zak's recurrence formulation to develop a finite element formulation and thereby improving the accuracy of solutions by exact integration of material properties under isothermal condition. Srinatha and Lewis[24] solved plane problems for isotropic materials using the trapezoidal integration method previously developed by Zak to evaluate integral equations. By using the direct integration scheme proposed by Taylor et al.,[23] the residual stresses and creep responses in unnotch/notched graphite/epoxy laminates are obtained by Lin and Hwang[25] and the time-dependent interlaminar stresses in GY70/339 composite laminates subjected to unit-step extensional loading are evaluated by Lin and Yi.[10] The accuracy of the direct integration schemes primarily depends upon the timestep size Δt. Therefore, use of the direct integration method for long time predictions of time-dependent dimensional changes and stresses in composite structures requires excessive amounts of computational time and memory since the solutions of rate-dependent problems at any time are influenced by all previous time solutions. Furthermore, numerical integration errors may be accumulated throughout the time history. Such error accumulations are described in detail in Refs. 18, 23, and 25.

In the present study, the integration of the finite element equilibrium equations is performed in the Laplace transform space rather than by direct time integrations. The advantages of this algorithm as compared to direct integration methods are accuracy of solutions, large computational time savings and decreased memory storage for the analysis of long time behavior, and significant decreases in labor needed to carry out numerical procedures and programming. Comparison studies between results of the present method and those of Refs. 10 and 23-25 using the direct time integration method were also presented in Refs. 17 and 18 for bending and stretching of composite plates.

For transient moisture and/or temperature distributions in viscoelastic bodies, the integral constitutive equations are not convolution ones and the approximate elastic-viscoelastic analogies[20,26] have been developed allowing the use of transform techniques. In the present analysis, the FEM equations are formulated in the real-time domain and then converted to reduced times, thereby not requiring any of the approximate formulations. Substituting Eq. (8) into Eq. (9) and taking the Laplace transform of the latter yields algebraic constitutive relationships. The transformed constitutive equations in the Laplace $s - x$ domain are

$$\tilde{\sigma}_i(x, s) = [\bar{Q}_{ij}^0 + \bar{Q}_{ij}^t s\tilde{f}(s)][\tilde{\epsilon}_j(x, s) - \tilde{\epsilon}_j^*(x, s)] \tag{28}$$

where $\sim$ denotes a Laplace transform and

$$\tilde{f}(s) = \sum_{\rho=1}^{N} \frac{\eta_\rho \lambda_\rho}{s\lambda_\rho + 1}$$

In the same manner, the finite element Eq. (27) are converted from hereditary integrals into algebraic ones, such that

$$[K_{mn}^0 + K_{mn}^t s\tilde{f}(s)]\tilde{U}_n(s) = \tilde{F}_m(s) + \tilde{F}_m^r(s) \tag{29}$$

One approach to solving the above system is to take an orthogonal transformation which simultaneously diagonalizes the two real and symmetric matrices K_{mn}^0 and K_{mn}^t.

The new nodal displacement vector $\{\tilde{U}'(s)\}$ is defined by

$$\{\tilde{U}'(s)\} = [\Phi]^T\{\tilde{U}(s)\} \tag{30}$$

where $[\Phi]$ is the orthogonal transformation matrix.

Substituting Eq. (30) into Eq. (29) and premultiplying by $[\Phi]^T$ results in a system of uncoupled algebraic relations:

$$[K_{mn}^{0'} + K_{mn}^{t'} s\tilde{f}(s)]\tilde{U}_n'(s) = \tilde{F}_m'(s) + \tilde{F}_m^{r'}(s) \tag{31}$$

where $K_{mn}^{0'} = \Phi_{pm}\Phi_{sn}K_{ps}^0$, $K_{mn}^{t'} = \Phi_{pm}\Phi_{sn}K_{ps}^t$, $\tilde{F}_m' = \Phi_{pm}\tilde{F}_p$, and $\tilde{F}_m^{r'} = \Phi_{pm}\tilde{F}_p^r$.

Note that the stiffness matrices $K_{mn}^{0'}$ and $K_{mn}^{t'}$ are now diagonalized. The orthogonal transformation matrix $[\Phi]$ can be evaluated by standard procedures such as the generalized Jacobi method.

The solution of the nodal displacements $U_n(s)$ is determined from Eqs. (30) and (31) in the Laplace domain and, by using numerical Laplace transform inversions in conjunction with Eq. (6), the displacements are transformed back into the real-time domain.

If the loading functions are provided in analytic forms, the partial-fraction method produces excellent results. Even if $\hat{F}_m(\zeta)$ and $\hat{F}_m^r(\zeta)$ are only presented numerically, a great number of numerical Laplace transform and numerical Laplace transform inversion techniques are available.[27-30] In Ref. 30, eight numerical algorithms of the Laplace transform inversion method are compared with each other indicating that Schapery's collocation method[27] and Cost and Becker's multidata method[28] provide good results for nonoscillatory functions of time with less needed computer time. Durbin's inversion method[29] based on Fast Fourier sine-cosine transformations yields accurate results for oscillatory time functions, however at the expense of much computing time. Considerable computing time can be saved if the inverse transformation is performed for only those degrees of freedom at nodes which are of primary interest.

After the displacement field is evaluated in the time domain, the time-dependent strains are calculated from Eqs. (2) and (14). The stresses in the Laplace domain are obtained from Eq. (28) and are then transformed into the time domain by using Eq. (6) and the Laplace transform inversion techniques previously discussed.

Failure Criterion for Delamination Onset

Brewer and Lagace[8] introduced the Quadratic Delamination Criterion to predict delamination initiation based upon free edge stress distributions. They report good agreement between results calculated by the Quadratic Delamination Criterion and experimental ones.

The time-dependent average stresses $\bar{\sigma}_i$ are defined as

$$\bar{\sigma}_i(t) = \frac{1}{x_{\text{avg}}} \int_{b - x_{\text{avg}}}^{b} \sigma_i(t)\, dx_2 \tag{32}$$

where b is half of the laminate width and x_{avg} is the averaging dimension or boundary width determined by experiments.

In the present study, the Quadratic Delamination Criterion is extended to take into account time-dependent creep rupture strengths by the following modification:

$$\left[\frac{\bar{\tau}_{xz}(t_d)}{Z_{xz}(t_d)}\right]^2 + \left[\frac{\bar{\tau}_{yz}(t_d)}{Z_{yz}(t_d)}\right]^2 + \left[\frac{\bar{\sigma}_z^{tn}(t_d)}{Z_z^{tn}(t_d)}\right]^2 + \left[\frac{\bar{\sigma}_z^{cm}(t_d)}{Z_z^{cm}(t_d)}\right]^2 = 1 \tag{33}$$

where

Z_z^{tn} = tensile creep rupture interlaminar normal strength in x_3 direction
Z_z^{cm} = compressive creep rupture interlaminar normal strength in x_3 direction

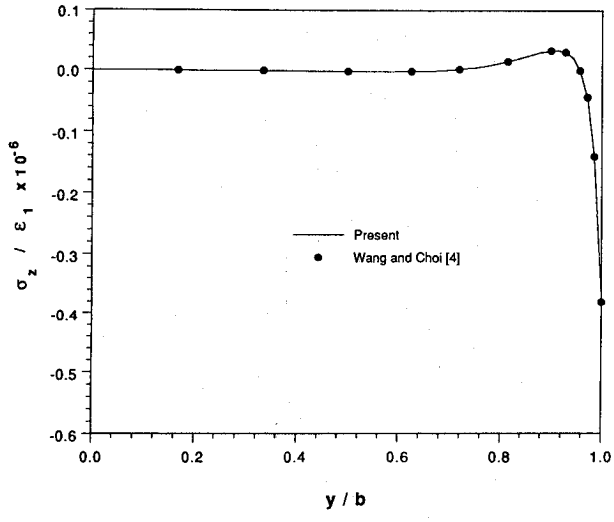

Fig. 2 Elastic interlaminar normal stresses along the interface in a $(45/-45)_s$ laminate.

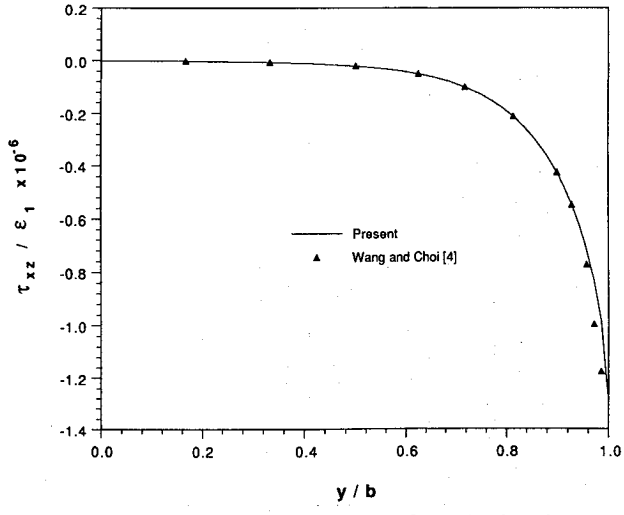

Fig. 3 Elastic interlaminar shear stresses along the interface in a $(45/-45)_s$ laminate.

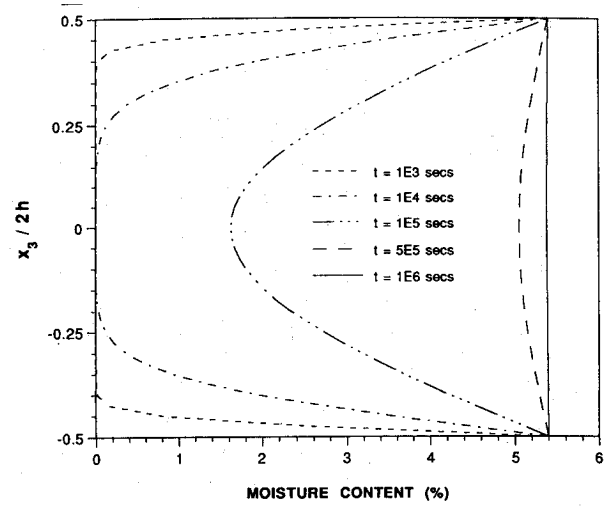

Fig. 4 Moisture distribution in a $(45/-45)_s$ kevlar/epoxy laminate ($T = 122°F$ and RH = 95%).

Z_{xz} = creep rupture interlaminar shear strength in x_1 and x_3 directions
Z_{yz} = creep rupture interlaminar shear strength in x_2 and x_3 directions
t_d = delamination onset failure time

Moisture Content Time Variations

Consider a thin laminate exposed to hygrothermal environments. The moisture distribution in the laminate thickness direction at a specific time can be found by solving a diffusion-type equation. The solution for the moisture concentration M then is[31]

$$\frac{M - M_0}{M_\infty - M_0} = 1 - \frac{4}{\pi} \sum_{j=0}^{\infty} \frac{1}{2j+1} \sin \frac{(2j+1)\pi(x_3 + h)}{2h} \cdot \exp\left[-\frac{(2j+1)^2 \pi^2 K^H t}{4h^2}\right] \tag{34}$$

where M_0 is the initial concentration at $t = 0$, M_∞ is the equilibrium moisture concentration at $t = \infty$, K^H is the moisture diffusion coefficient, and $2h$ is the laminate thickness.

The average moisture content $\bar{M}$ through the laminate thickness can be expressed as

$$\bar{M} = \frac{1}{2h} \int_{-h}^{h} M\, dx_3 \tag{35}$$

and then the average moisture concentration at any specific time t reduces to

$$\frac{\bar{M} - M_0}{M_\infty - M_0} = 1 - \frac{8}{\pi^2} \sum_{j=0}^{\infty} \frac{1}{(2j+1)^2} \cdot \exp\left[-\frac{(2j+1)^2 \pi^2 K^H t}{4h^2}\right] \tag{36}$$

Numerical Results and Discussion

To verify the present analysis, free edge stresses at $t = 0$ evaluated by the present formulation are compared with the exact elastic solutions obtained by Wang and Choi.[5] The $(45/-45)_s$ laminate was subjected to the uniaxial strain $\epsilon_1 = 10^{-6}$ in./in. A total of 280 elements with 957 degrees of freedom (DOF) were used and the generalized Jacobi method was adopted to find an orthogonal transformation matrix. The interlaminar stresses σ_z and τ_{xz} are depicted in Figs. 2 and 3, which show excellent agreement between the two solutions.

Several studies were conducted to analyze the time-dependent responses near the free edges of laminated composites. The effects of degradation of material properties, layup orientations, and severe environmental conditions on thermal and

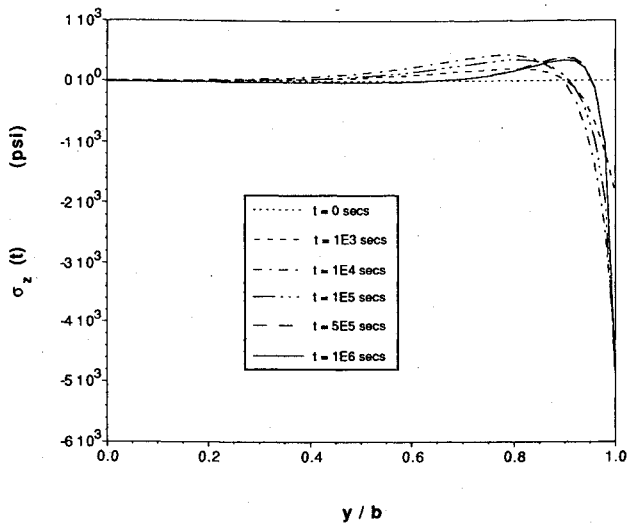

Fig. 5 Time-dependent interlaminar normal stress σ_z in $(45/-45)_s$ kevlar/epoxy laminate ($x_3 = 0.058$ in.).

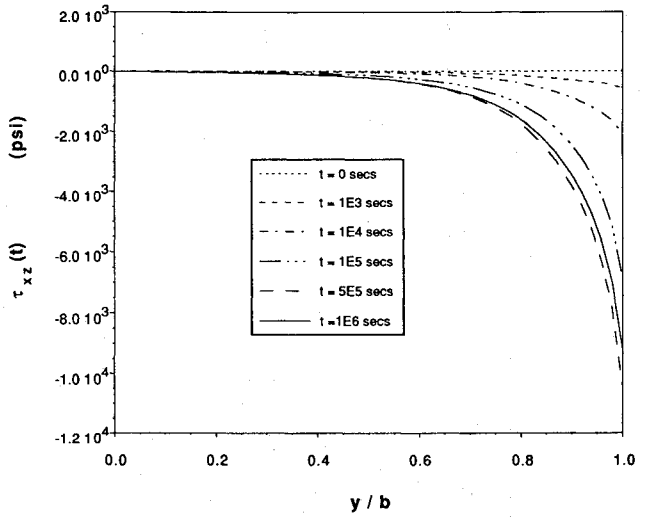

Fig. 6 Time-dependent interlaminar shear stress τ_{xz} in $(45/-45)_s$ kevlar/epoxy laminate ($x_3 = 0.058$ in.).

hygroscopic edge stresses have also been evaluated. In the present study, kevlar/epoxy and T300/934 composites were considered. The same number of elements as those involved in the $t = 0$ verification study was also used to calculate the time-dependent boundary-layer stresses and strains. The laminate width-to-thickness ratio is four and the ply thickness is 0.0058 in. The experimentally determined viscoelastic material properties for T300/934 graphite/epoxy and kevlar/epoxy composite laminates are presented in Refs. 11 and 34, respectively, and their master relaxation modulus curves and shift functions were used.

Under isothermal conditions, time-dependent stress singularities near free edges of kevlar/epoxy composite laminates with $(45/-45)_s$ layups subjected to moisture absorption were calculated. Moisture is well known to significantly affect the stiffnesses and strength of kevlar/epoxy composites making hygroscopic boundary-layer stresses in kevlar/epoxy laminates very interesting. Moisture content in a laminate is a function of time, temperature, and laminate thickness. The initial environmental condition for a laminate was taken as 122°F/0% relative humidity (RH), and initial moisture content in each laminate as 0%. These conditions changed to 122°F/95% RH instantly at time $t = 0^+$. The laminate then absorbed moisture for a 10^6-s period at the end of which its moisture content reached equilibrium conditions. The reduced time was approximated by secants which was formulated for the elastic-viscoelastic analogy in Ref. 35. The moisture gradient as a function of time in such a laminate is depicted in Fig. 4. The time variations of the moisture induced stresses σ_z and τ_{xz} at the interface between 45 deg and -45 deg layers were

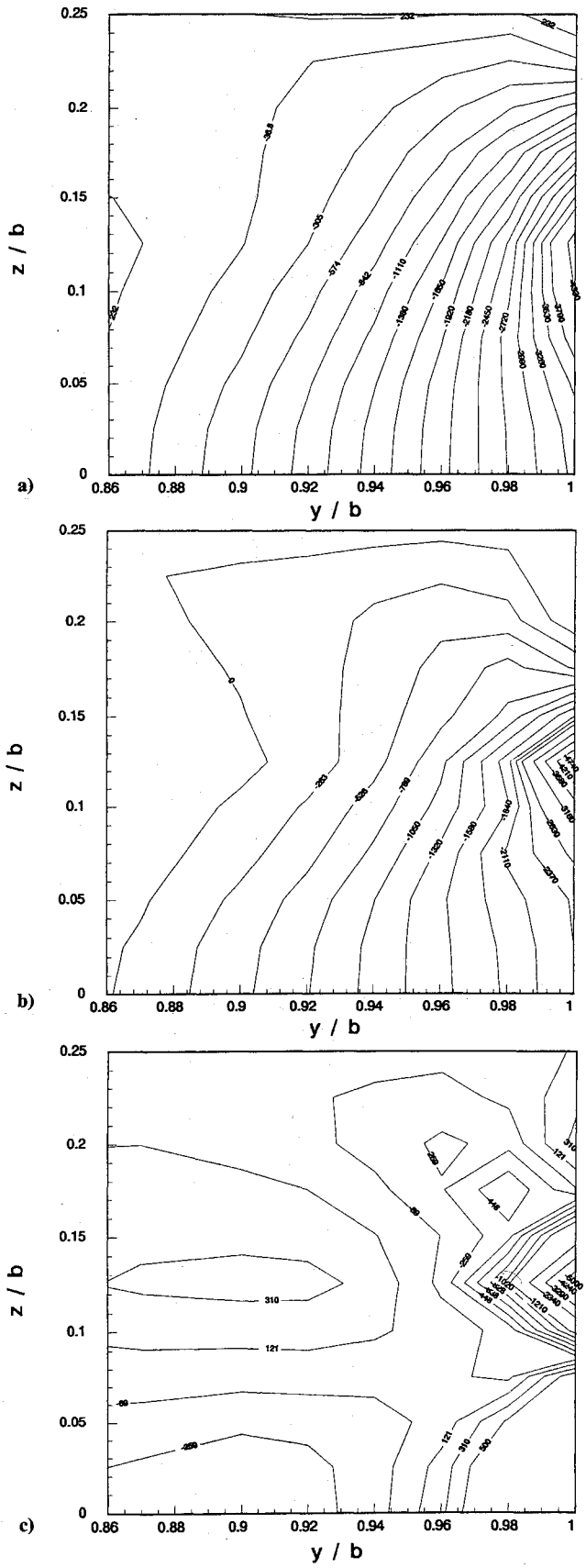

Fig. 7 Time-dependent interlaminar normal stress σ_z near the free edge of $(45/-45)_s$ kevlar/epoxy laminate at various times: a) $t = 10^4$ s, b) $t = 10^5$ s, and c) $t = 5 \times 10^5$ s.

evaluated and are illustrated in Figs. 5 and 6, respectively. The stresses increased with moisture absorption and the stresses developed by a hygroscopic loading were much larger than the loss due to relaxation (up to $t = 5 \times 10^5$ s). However, the magnitudes of stresses σ_z and τ_{xz} at $t = 5 \times 10^5$ s also were larger than those at $t = 10^6$ s since these stresses were relaxing during that moisture absorption period. Appreciable stress relaxation occurred before the equilibrium moisture content was reached. Such relaxation resulted in decreasing the magnitude of residual stresses. The moisture-induced interlaminar stresses σ_z and τ_{xz} near the free edge of a laminate are contour-plotted at various times in Figs. 7 and 8, respectively. Figure 7

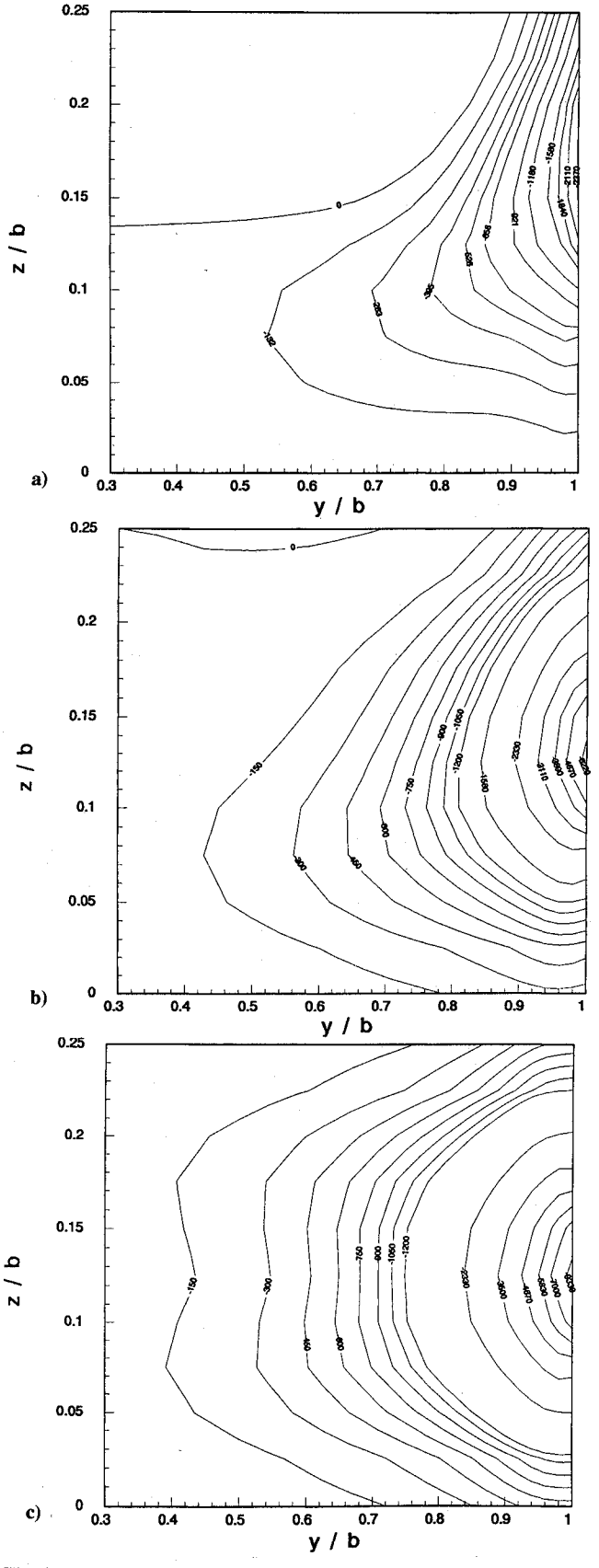

Fig. 8 Time-dependent interlaminar shear stress τ_{xz} near the free edge of $(45/-45)_s$ kevlar/epoxy laminate at various times: a) $t = 10^4$ s, b) $t = 10^5$ s, and c) $t = 5 \times 10^5$ s.

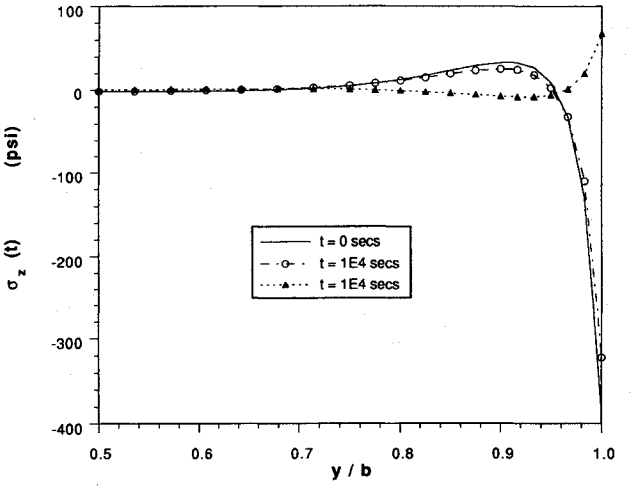

Fig. 9 Time-dependent interlaminar normal stress in $(45/-45)_s$ T300/934 graphite/epoxy laminate ($x_3 = 0.058$ in.).

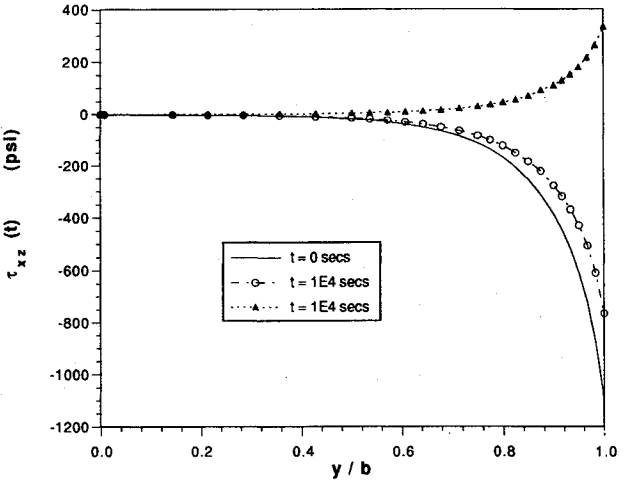

Fig. 10 Time-dependent interlaminar shear stress in $(45/-45)_s$ T300/934 graphite/epoxy laminate ($x_3 = 0.058$ in.).

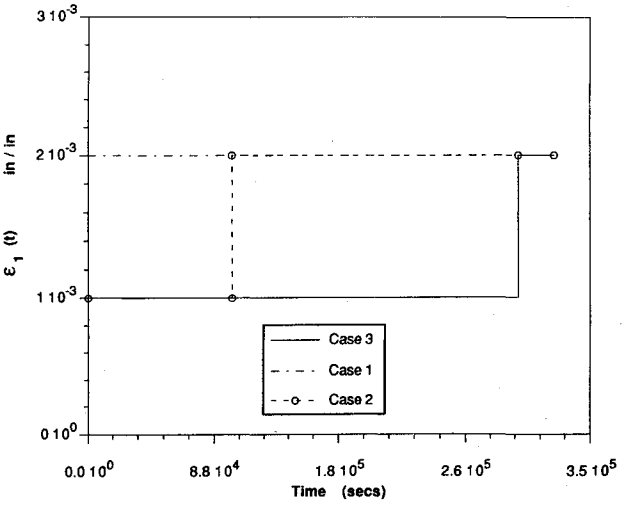

Fig. 11 Extensional loads for $(15/-15)_s$ T300/934 graphite/epoxy laminates.

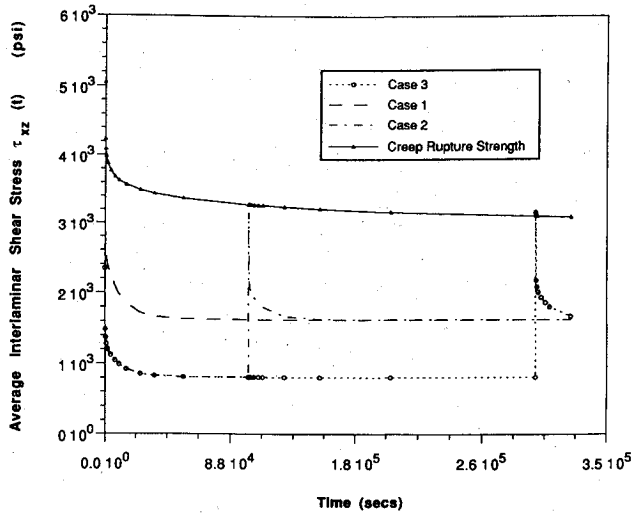

Fig. 12 Average interlaminar shear stresses in $(15/-15)_s$ T300/934 graphite/epoxy laminates.

shows that the interlaminar normal stress σ_z was significantly developed near the free edge of the 45 deg and -45 deg interface during the loading period. Time-dependent interlaminar shear stress concentrations are also shown in Fig. 10. It is believed that those stress singularities are responsible for the delamination of a laminate. From $t = 10^4$ to 5×10^6 s, the magnitude of τ_{xz} increased by about 434% near the free edge ($x_3 = 0.0058$ in., $y/b = 0.99$) during the moisture absorption period while σ_z increased by only 12%. The results showed that the magnitudes of the time-dependent interlaminar stresses σ_z and τ_{xz} near the free edge of the 45 deg and -45 deg interface were much larger than those elsewhere for the entire loading period.

A second study was conducted for a $(45/-45)_s$ T300/934 graphite/epoxy composite laminate subjected to uniaxial loads under isohygrothermal conditions ($T = 140°F$ and RH = 0%). The time-dependent interlaminar stresses for $(45/-45)_s$ laminates subjected to extensional loading were calculated. A step loading was used by applying a strain $\epsilon_1 = 0.005$ in./in. which was held constant for 1 month and then removed in an instantaneous elastic step. The time-dependent interlaminar stresses σ_z and τ_{xz} along the interface between 45 deg and -45 deg layers are plotted in Figs. 9 and 10. Over the loading period, stress relaxation occurred and the sign of stresses changed after the loading was removed. This case illustrates that residual stresses may exist in viscoelastic composite laminates even though the laminate is no longer subjected to any loading.

Another study involved the prediction of delamination initiation as a function of loading history. Prediction of delamination onset for a viscoelastic composite material requires the development of a time-dependent failure criterion since stresses and strains depend on loading histories. In this paper, the Quadratic Delamination Criterion was extended to account for time-dependent creep rupture strengths; see Eq. (33). Because no experimental data for the creep rupture interlaminar strengths of composite laminates were available, the creep rupture transverse and shear strengths of T300/934 graphite/epoxy composites were used for $Z_z^{in}(t)$ and $Z_{xz}(t)$. These were determined experimentally and are given in Ref. 32. The averaging dimension x_{avg} was taken as 0.145 mm in the same manner as in Ref. 8.

The loading histories for three uniaxial loading cases applied to $(15/-15)_s$ laminates are plotted in Fig. 11. The magnitude of loading was identical in each case, but the applied times were different. The $(15/-15)_s$ layups of T300/934 composite laminates were studied. The interlaminar shear stress was dominant at the free edges, and this stress is believed to be responsible for laminate failures. The time-dependent average interlaminar shear stresses are plotted in Fig. 12 by using Eq. (28). In cases 1 and 2, no initiation of delaminations were observed. However, in case 3, delamination initiation occurred at the free edge of the interface between 15 deg and -15 deg layers at $t = 3 \times 10^5$ s since the creep rupture strength of laminates were decreasing with increasing time.

Conclusions

Numerical results indicate that the time-dependent interlaminar stresses and strains for a given geometry and epoxy matrix composite are significantly influenced by temperature, moisture content, and loading history. When the laminate is subjected to a step extensional load, time-dependent interlaminar stresses relax during the loading period and residual stresses remain after the load is removed. The residual stresses are evaluated by viscoelastic analysis and from known loading histories, and these stresses are accumulated throughout the loading and unloading cycles. Because of the presence of residual stresses and decreased creep rupture strengths, the laminate may fail under loads which are considerably lower than the corresponding elastic critical strengths. The initiation of delamination in epoxy matrix composite laminates can be predicted by the newly developed modified Quadratic Delamination Criterion. The present studies show that the delamination onset in viscoelastic composites depends not only on the loading magnitude but also on the loading history.

Acknowledgments

This work was supported in part by a grant from the IBM Palo Alto Scientific Center. The author wishes to express his sincere gratitude to Harry H. Hilton in the Department of Aeronautical and Astronautical Engineering at the University of Illinois at Urbana-Champaign and to Kuen Y. Lin in the Department of Aeronautics and Astronautics at the University of Washington for their support, academic guidance, and encouragement throughout this study.

References

[1]Pipes, R. B., and Pagano, N. J., "Interlaminar Stresses in Composite Laminates Under Uniform Axial Extension," *Journal of Composite Materials*, Vol. 4, Oct. 1970, pp. 538–548.

[2]Wang, A. S. D., and Crossman, F. W., "Edge Effects on Thermally Induced Stresses in Composite Laminates," *Journal of Composite Materials*, Vol. 11, Jan. 1977, pp. 300,301.

[3]O'Brien, T. K., "Characterization of Delamination Onset and Growth in a Composite Laminates," *Damage in Composite Materials, ASTM STP 775*, American Society for Testing and Materials, Philadelphia, PA, 1982, pp. 140–167.

[4]Wang, S. S., and Choi, I., "Boundary-Layer Effects in Composite Laminates: Part 2—Free Edge Stress Solutions and Basic Characteristics," *Journal of Applied Mechanics*, Vol. 49, Sept. 1982, pp. 541–548.

[5]Wang, S. S., and Choi, I., "Influence of Fiber Orientation and Ply Thickness on Hygroscopic Boundary-Layer Stresses in Angle-Ply Composite Laminates," *Journal of Composite Materials*, Vol. 16, Sept. 1982, pp. 244–256.

[6]Kim, R. Y., and Soni, S. R., "Experimental and Analytical Studies On the Onset of Delamination in Laminated Composites," *Journal of Composite Materials*, Vol. 18, Jan. 1984, pp. 70–80.

[7]Sun, C. T., and Chen, J. K., "Effect of Plasticity on Free Edge Stresses in Boron-Aluminum Composite Laminates," *Journal of Composite Materials*, Vol. 21, Oct. 1987, pp. 969–985.

[8]Brewer, J. C., and Lagace, P. A., "Quadratic Stress Criterion for Initiation of Delamination," *Journal of Composite Materials*, Vol. 22, Dec. 1988, pp. 1141–1155.

[9]Bouadi, H., and Sun, C. T., "Hygrothermal Effects on the Stress Field of Composites," *Journal of Reinforced Plastics and Composites*, Vol. 8, Jan. 1989, pp. 40–54.

[10]Lin, K. Y., and Yi, S., "Analysis of Interlaminar Stresses in Viscoelastic Composites," *International Journal of Solids and Structures*, Vol. 27, No. 7, 1991, pp. 929–945.

[11]Crossman, F. W., Mauri, R. E., and Warren, W. J., "Moisture Altered Viscoelastic Response of Graphite/Epoxy Composite," *Advanced Composite Materials—Environmental Effects, ASTM STP 658*, edited by J.R. Vinson, Philadelphia, PA, 1978, pp. 200–205.

[12]Kibler, K. G.,"Effects of Temperature and Moisture on the Creep Compliance of Graphite-Epoxy Composites," *Effect of Service Environment on Composite Materials,* AGARD-CP-288, Neuilly Sur Seine, France, 1981.

[13]Tuttle, M. E., and Brinson, H. F., "Prediction of the Long-Term Creep Compliance of General Composite Laminates," *Experimental Mechanics*, Vol. 26, No. 1, 1986, pp. 89–102.

[14]Flaggs, D. L., and Crossman, F. W., "Analysis of the Viscoelastic Response of Composite Laminates During Hygrothermal Exposure," *Journal of Composite Materials*, Vol. 15, Jan. 1981, pp. 21–40.

[15]Harper, B. D., and Weitsman, Y., "On the Effects of Environmental Conditioning on Residual Stresses in Composite Laminates," *International Journal of Solids and Structures*, Vol. 21, No. 8, 1985, pp. 907–926.

[16]Whiteside, J. B., DeIasi, R. J., and Schulte, R. L., "Distribution of Absorbed Moisture in Graphite/Epoxy Laminates After Real Time Environmental Cycling," *Long-Term Behavior of Composites, ASTM STP 813*, edited by T. K. O'Brien, American Society for Testing and Materials, Philadelphia, PA, 1983, pp. 192–205.

[17]Hilton, H. H., and Yi, S., "Anisotropic Viscoelastic Finite Element Analysis of Mechanically and Hygrothermally Loaded Composites," *Composites Engineering*, Vol. 3, No. 2, 1993, pp. 123–135.

[18]Hilton, H. H., and Yi, S., "Bending and Stretching Finite Element Analysis of Anisotropic Viscoelastic Composite Plates," *Proceedings of Third Air Force/NASA Symposium on Recent Advances in Multidisciplinary Analysis and Optimization* (San Francisco, CA), Sept. 1990, pp. 488–494.

[19]Hilton, H. H., "Viscoelastic Analysis," *Engineering Design for Plastics*, Reinhold, New York, 1964, pp. 199–276.

[20]Hilton, H. H., and Dong, S. B., "An Analogy for Anisotropic, Nonhomogeneous, Linear Viscoelasticity Including Thermal Stresses," *Proceedings of 8th Midwestern Mechanics Conference* (Cleveland, OH), May 1964, pp. 58–73.

[21]Gurtin, M. E., "Variational Principles in the Linear Theory of Viscoelasticity," *Archive Rational Mechanics and Analysis*, Vol. 13, 1963, pp. 179–185.

[22]Zak, A. R.,"Structural Analysis of Realistic Solid Propellant Materials," *Journal of Spacecraft and Rockets*, Vol. 5, No. 3, 1967, pp. 270–275.

[23]Taylor, R. L., Pister, K. S., and Goudreau, G. L., "Thermomechanical Analysis of Viscoelastic Solids," *International Journal for Numerical Methods in Engineering*, Vol. 2, No. 1, 1970, pp. 45–59.

[24]Srinatha, H. R., and Lewis, R. W., "A Finite Element Method for Thermoviscoelastic Analysis of Plane Problems," *Computer Methods in Applied Mechanics and Engineering*, Vol. 25, 1981, pp. 21–33.

[25]Lin, K. Y., and Hwang, I. H., "Thermo-Viscoelastic Analysis of Composite Materials," *Journal of Composite Materials*, Vol. 23, June 1989, pp. 554–569.

[26]Hilton, H. H., and Russell, H. G., "An Extension of Alfrey's Analogy to Thermal Stress Problems in Temperature-Dependent Linear Viscoelastic Media," *Journal of Mechanics and Physics of Solids,* Vol. 9, July 1961, pp. 152–164.

[27]Schapery, R. A., "Approximate Methods of Transform Inversion for Viscoelastic Stress Analysis," *Proceedings of 4th U.S. National Congress on Applied Mechanics,* American Society of Mechanical Engineers, New York, June 1962, pp. 1075–1085.

[28]Cost, T. L., and Becker, E. B., "A Multidata Method of Approximate Laplace Transform Inversion," *International Journal for Numerical Methods in Engineering*, Vol. 2, No. 2, 1970, pp. 207–219.

[29]Durbin, F., "Numerical Inversion of Laplace Transforms: An Efficient Improvement to Dubner and Abate's Method," *The Computer Journal*, Vol. 17, No. 4, 1974, pp. 371–376.

[30]Narayanan, G. V., and Beskos, D. E., "Numerical Operational Methods for Time-Dependent Linear Problems," *International Journal for Numerical Methods in Engineering*, Vol. 18, No. 12, 1982, pp. 1829–1854.

[31]Tsai, S. W., and Hahn, H. T., *Introduction to Composite Materials*, Technomic, Westport, CT, 1980, Chap. 8.

[32]Dillard, D. A., and Brinson, H. F., "A Numerical Procedure for Predicting Creep and Delayed Failure in Laminated Composites," *Long-Term Behavior of Composites, ASTM STP 813*, edited by T. K. O'Brien, Philadelphia, PA, 1983, pp. 23–37.

[33]Whitney, J. M., and Nuismer, R. J., "Stress Fracture Criteria for Laminated Composites Containing Stress Concentrations," *Journal of Composite Materials*, Vol. 8, 1974, pp. 253–265.

[34]Yi, S., "Time Dependent Behaviors of Composite Laminates in Hygrothermal Environment," M.S. Thesis, Dept. of Aeronautics and Astronautics, Univ. of Washington, Seattle, WA, June 1987.

[35]Hilton, H. H., and Clements, J. R., "Formulation and Evaluation of Approximate Analogies for Transient Temperature Dependent Linear Viscoelastic Media," *Proceedings of the Conference on Thermal Loading and Creep* (London), May 1964, pp. 6:17–6:24.